A comparison of power controlled flash sintering and conventional sintering of strontium titanate

Fabian Lemke, Wolfgang Rheinheimer and Michael J. Hoffmann

Abstract

The microstructural evolution of $SrTiO_3$ is analyzed during power controlled flash sintering. A controllable sintering process is achieved by lowering the specific power densities yielding a relatively slow flash sintering. The analytical equations for sintering developed by Coble are used to characterize flash sintering. The focus is on the evolution of microstructure obtained by the observation by different heating times compared to conventional sintering. The results are discussed in comparison to conventional sintering and the impact of joule heating and to the current state of research on flash sintering of ZrO_2.

Keywords

Flash sintering; electric field assisted sintering; strontium titanate; Joule heating

Since the first appearance of flash sintering, ZrO_2 was used as a model material to understand the acceleration of sintering in electric fields and with electric currents [1-7]. Aspects like joule heating, a change of the defect chemistry and structural lattice changes are considered to cause the fast densification of zirconia [8-10]. Nevertheless flash sintering is not yet fully understood for zirconia; for other material classes even less information is available. For perovskites as $SrTiO_3$ a change of the defect chemistry or of the crystal structure seems not to occur [11].

Apparently joule heating is of significant impact during flash sintering of all materials. Its impact on the sample temperature during flash sintering was investigated in vast detail and is generally well understood [9, 12], although there may be effects due to local overheating at particle necks and, thus, internal temperature distribution in the sample. The sample temperature T_{calc} during flash sintering was obtained under consideration of the black body radiation [9]

$$\frac{T_{calc}}{T_{meas}} = \left[1 + \frac{1000 \cdot W_V}{\sigma \cdot T_{meas}^4} \cdot \left(\frac{V}{A}\right)\right]^{1/4} \quad (1)$$

with the measured sample temperature T_{meas}, the volumetric power dissipation of the sample W_V, the volume to area ratio V/A and a universal physical constant $\sigma = 5.67 \cdot 10^{-8}\, Wm^2K^{-4}$.

The microstructural evolution during flash sintering is hard to observe since densification is very fast and quenching from a setup with electric contacts is experimentally difficult. In this study we present a method where the samples undergo a relatively slow flash sintering process with low current and power densities. By limiting the power source output, densification remains controllable and proceeds within a few minutes. The densification process is analyzed analogue to conventional sintering using the well-known Coble model [13-15]. A simplified equation for the densification rate $\dot{\rho}$ is given by

$$\dot{\rho} = C \cdot D/G^m \qquad 2$$

where C is a constant, D is the diffusion coefficient and G is the mean grain diameter. The exponent m depends on the dominating diffusion mechanism ($m = 3$ for volume diffusion and $m = 4$ for grain boundary diffusion).

High purity strontium titanate powder was prepared by the mixed oxide/carbonate route using $SrCO_3$ and TiO_2 (purities of 99.95 and 99.995%, respectively, Sigma Aldrich Chemie GmbH, Taufkirchen, Germany). The Sr/Ti ratio was 0.996. Cylindrical green bodies were uniaxially pressed (6 mm long and 8 mm in diameter) in a steel die and subsequently cold-isostatically pressed at 400 MPa. Geometric green densities were found to be 63±1%.

Flash sintering experiments were conducted in an optical dilatometer (TOMMI plus, Fraunhofer ISC, Germany). Samples were contacted with platinum wire spirals as electrodes and platinum wires as cables. The furnace was heated to 1120 °C or 1150 °C. After 10 minutes of equilibration time an electrical field was applied to the samples (XG 600-2.8, Ametek, United States). The field was limited to 500 V/cm, but for all experiments reported here this field was reached only initially, since the high conductivity of the samples resulted in current-controlled output. The current limit I_{max} was varied to limit and control the power dissipation of the sample. The power density is assumed to be

$$P_V = \frac{U \cdot I}{V} \qquad 3$$

with the voltage U applied to the sample, the current I flowing through the sample and the sample volume V. As will be shown later, the powder dissipation reached a steady state

within short times. In the present experiments the maximum power density was ~100 mW/mm².

Sintered samples were prepared for SEM imaging to observe microstructures. Polished samples were thermally etched at 1075 °C for 2 h. The average grain size was obtained by the line intersection method observing more than 500 grains per sample (AnalySis Software, Olympus, Japan).

Table 1 gives the furnace and power source conditions as well as the measured and estimated true sample temperature. The measured sample temperature refers to a thermocouple close to the sample. A comparison of the furnace temperature $T_{furnace}$ and the measured sample temperature T_{meas} shows that increasing current limits result in significant joule heating of the sample. However, T_{meas} cannot give the true temperature of a sample that is heated by joule heating. Thus Eqn. 1 was used to estimate the true sample temperature T_{calc} needed for a comparison with conventional sintering. Accordingly the temperature increase by joule heating is $\Delta T = T_{calc} - T_{furnace}$.

$T_{furnace}$	I_{max}	T_{meas}	T_{calc}	ΔT
1120°C	**120mA**	**1170°C**	**1240°C**	**120°C**
1150°C	**100mA**	**1180°C**	**1190°C**	**40°C**
1150°C	**200mA**	**1190°C**	**1275°C**	**125°C**
1150°C	**500mA**	**1200°C**	**1345°C**	**195°C**

Table 1: Current limit, furnace temperature, measured and calculated sample temperature and estimated temperature increase of the sample by joule heating (see text for details).

For a set of isothermal experiments (1150 °C, I_{max} = 100mA to 500mA) the power density and the shrinkage L/L_0 are shown in Figure 1. As the field is applied, the high conductivity of the material results in current controlled output within a few minutes. At a furnace temperature of 1150°C, the power density reaches a steady state for I_{max} = 100mA. For 200mA, the power density almost reaches a steady state as well, but with significant instability (i.e. scattering and slight increase with time). However, for 500mA a very unstable powder density is evident: strong scattering occurs along with a significant increase with time.

The linear shrinkage strongly depends on the power density. For 500 mA the sample densifies within 5 minutes. However, after densification the sample slightly elongates with

time. A comparison with the power density (which also increases with time) suggests that the sample temperature increases and thermal expansion occurs. For 100 mA and 200 mA, densification is slower and very similar to conventional sintering behavior [16].

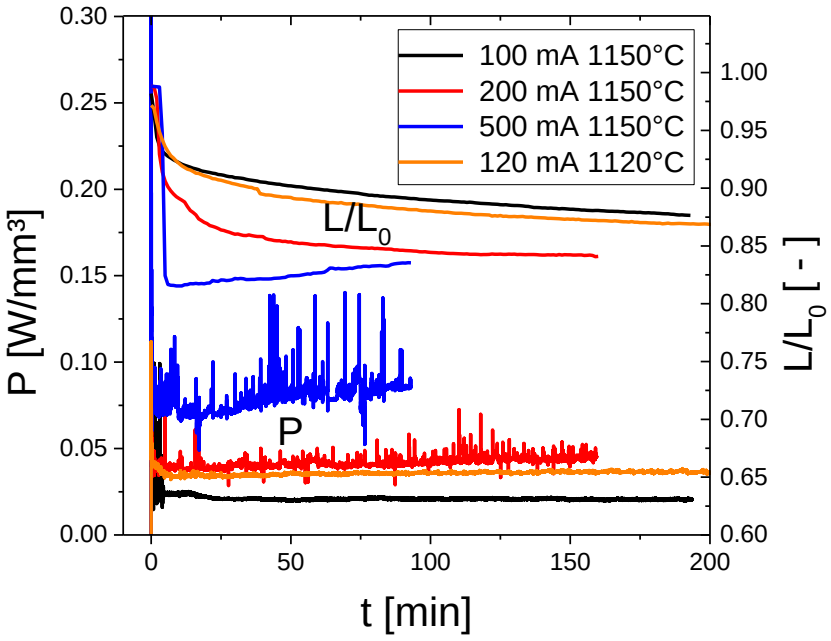

Figure 1 power densities and linear shrinkage during power controlled flash sintering for three different current limits. The furnace temperature was 1150°C for 100mA, 200mA and 500mA and 1120°C for 120mA.

Since a comparison of field assisted sintering and conventional sintering requires stable experimental conditions (i.e. constant power dissipation at the sample), the furnace temperature was decreased and the current limit increased to find a set of parameters, which results in stable power dissipation but with significant joule heating. At a furnace temperature of 1120°C and a current limit of 120mA, very stable power dissipation was reached with an estimated sample temperature of 1240°C (cf. Figure 1 and Table 1). The resulting field at the sample was ~80V/mm. This dataset was chosen for a detailed comparison to conventional field-free sintering at 1280°C [16].

The densification for conventional sintering at 1280°C and for field assisted sintering at T_{calc} = 1240°C (I_{max} = 120mA) is shown in Figure 2a. For both experiments several curves are shown indicating different heating times. In general, both experimental setups show very similar densification. For field assisted sintering the densification is slightly slower than for

conventional sintering, but given the estimated temperature difference of 40K this is to be expected (conventional sintering at 1280°C and field assisted sintering at 1240°C).

For both setups the mean grain size was measured after different heating times (cf. Figure 2b). Again both setups give very similar results with the field assisted sintering having slightly smaller grain sizes, most likely for the same reason as the slower densification. Fig. 3 shows microstructures after 30 min and 120 min for field assisted and conventionally sintered samples. Besides minor differences in porosity and grain size the microstructures are very similar. The small variance in density and grain size is again most likely attributed to the temperature difference of 40K.

A standard grain growth law was fitted to the grain growth data in Figure 2b to compare grain growth during field assisted and conventional sintering [17]:

$$\mathrm{G}^2 - G_0^2 = k \cdot t \qquad 4$$

with the mean grain diameter G, the mean diameter G_0 at time $t = 0$ and the grain growth constant k. A grain growth constant of $k = 4.9 \cdot 10^{-17}\ m^2/s$ was obtained for the power controlled samples; for conventional sintering $k = 6.6 \cdot 10^{-17}\ m^2/s$ was found. These values are very similar and agree well with previously reported results for grain growth during final stage sintering [16]. Even grain growth in dense polycrystals gives very similar results [18-20] indicating that pore drag plays no particular role for grain growth in strontium titanate [21, 22]. Therefore, an influence on the sintering process due to drastic changes in grain growth or grain and pore morphology seems to be unlikely.

A recent study observed grain growth in dense strontium titanate in the no-current case (i.e. with insulating electrodes) [23]. In these experiments, a gradient of the grain growth rate along the electric field was found. This gradient seems to be caused by defect redistribution across the samples by the electric field. However, this gradient was very weak below 1460°C and since the present experiments were below 1300°C, no significant gradient is expected. In the present experiments no changes or gradients of the microstructure across the sample were found.

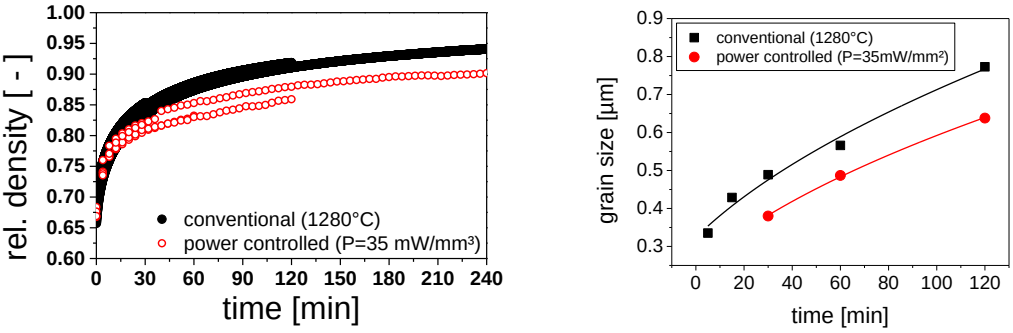

Figure 2 relative density of power controlled flash sintering with 35mW/mm³ at a furnace temperature of 1120°C compared to conventional sintering at 1180°C (a). Evolution of the grain size during sintering for power controlled flash sintering and conventional sintering at 1180°C (b).

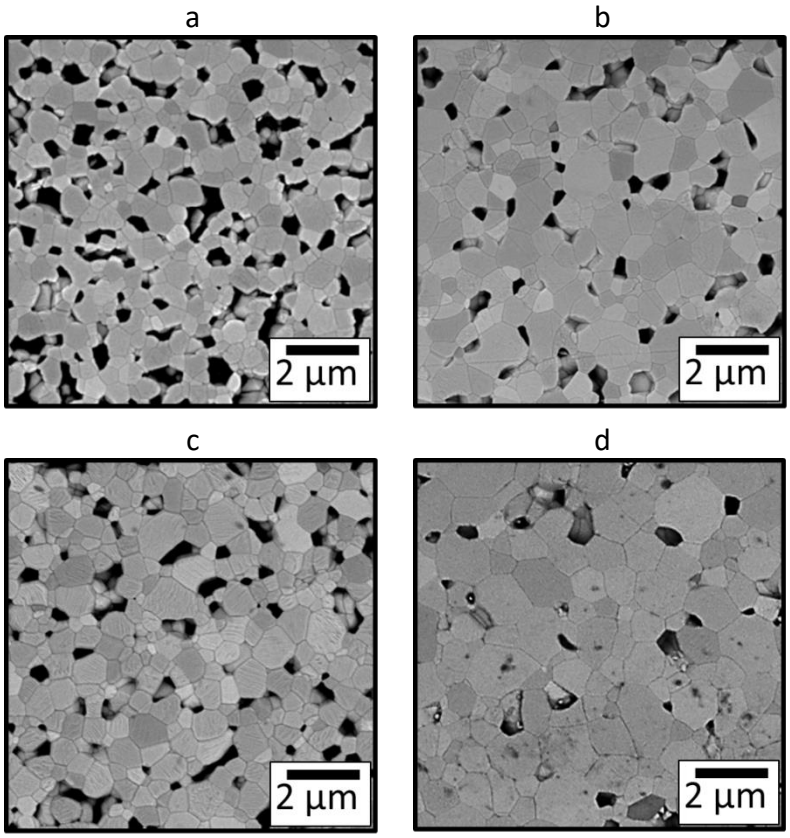

Figure 3 microstructures after 30min (a) and 120min (b) for power controlled flash sintering with 35mW/mm³ at a furnace temperature of 1120°C and after 30min (c) and 120min (d) for conventional sintering at 1180°C.

The densification rate of both setups is shown in Figure 4 with respect to mean grain size. As in Figure 2, the slightly lower densification rates for field assisted sintering are most likely caused by the slightly lower temperature (estimated temperature difference of 40K). Nevertheless, the densification characteristic is very similar during the entire sintering process. **Fehler! Verweisquelle konnte nicht gefunden werden.**Figure 4 allows evaluating the dominating diffusion mechanism during sintering by observing the slope of a fit of equation 2 to the sintering rate. For conventional sintering, m = 3.8 was obtained indicating grain boundary diffusion as dominant transport mechanism [16]. The field assisted sintering data yield the same result (m = 4). Accordingly, the presence of an electric field does not change the diffusion mechanism by which sintering occurs.

Very different conclusions were found for the binary compounds zirconia and titania: defect chemical and structural changes were argued to occur during flash sintering [8, 9, 24-26]. In particular a creation of vacancies and interstitial point defects was discussed to explain the massive diffusion during flash sintering of zirconia [8, 24, 27]. However, this mechanism should increase the bulk diffusivity more than the grain boundary diffusion, since it is a volume effect. If a similar effect would occur in the present experiment, the slope of the flash sintering curve in Figure 4 should indicate a slope of or close to three, which is not the case. Accordingly the defect chemistry of strontium titanate seems not to change drastically in the present experimental setup.

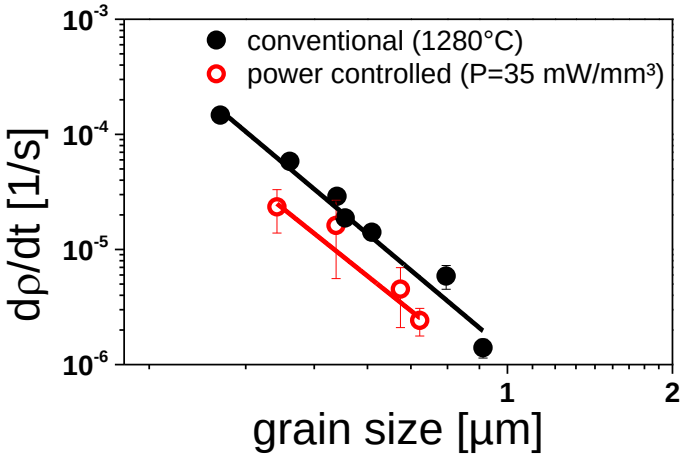

Figure 4 densification rate with respect to grain size for power controlled flash sintering with 35mW/mm³ at a furnace temperature of 1120°C and for conventional sintering at 1180°C.

Overall, power controlled flash sintering and conventional sintering are very similar as shown in Figure 2, Figure 3 and Figure 4 and as discussed above. This conclusion bases on (1) the similarity of densification curves, (2) microstructures (porosity, grain size and grain growth constants) and (3) the dominating diffusion mechanism during sintering. No significant difference seems to arise by the presence of an electric field of ~80V/mm. The assumption of joule heating alone is sufficient to understand the presented experiments. However, the presented experimental setup of a power controlled flash sintering with low power densities (~35mW/mm³) and electric fields (~80V/mm) shows that flash sintering can be a well controllable process.

Acknowledgement

This work was partially funded by the DFG within the SPP1959 under contract HO 1165/20-1.

References

[1] Cologna M, Prette ALG, Raj R. J Am Ceram Soc 2011;0pt94:316.

[2] Cologna M, Rashkova B, Raj R. J Am Ceram Soc 2010;0pt93:3556.

[3] Francis JSC, Raj R. J Am Ceram Soc 2012;0pt95:138.

[4] Francis JSC, Raj R. J Am Ceram Soc 2013;0pt96:2754.

[5] Francis JSC, Cologna M, Raj R. J Eur Ceram Soc 2012;0pt32:3129.

[6] Majidi H, van Benthem K. Physical Review Letters 2015;0pt114:195503.

[7] Majidi H, Holland TB, van Benthem K. Ultramicroscopy 2015;0pt152:35.

[8] Lebrun JM, Morrissey TG, Francis JSC, Seymour KC, Kriven WM, Raj R. Journal of the American Ceramic Society 2015;0pt98:1493.

[9] Raj R. J Eur Ceram Soc 2012;0pt32:2293.

[10] Terauds K, Lebrun JM, Lee HH, Jeon TY, Lee SH, Je JH, Raj R. Journal of the European Ceramic Society 2015;0pt35:3195.

[11] Karakuscu A, Cologna M, Yarotski D, Won J, Francis JSC, Raj R, Uberuaga BP. J Am Ceram Soc 2012;0pt95:2531.

[12] da Silva JGP, Lebrun JM, Al-Qureshi HA, Janssen R, Raj R. Journal of the American Ceramic Society 2015;0pt98:3525.

[13] Coble RL. J Appl Phys 1961;0pt32:787.

[14] Coble RL. J Appl Phys 1961;0pt32:793.

[15] Coble RL. Journal of Applied Physics 1965;0pt36:2327.

[16] Lemke F, Rheinheimer W, Hoffmann M. Journal of Ceramic Society of Japan 2016;0pt124:346.

[17] Burke JE, Turnbull D. Progress in Metal Physics 1952;0pt3:220.

[18] Rheinheimer W, Hoffmann MJ. Current Opinion in Solid State and Materials Science 2016;0pt20:286 . Grain boundary complexions -current status and future directions.

[19] Rheinheimer W, Hoffmann M. Journal of Materials Science 2015;0ptHTC 2015:1.

[20] Rheinheimer W, Hoffmann MJ. Scr Mater 2015;0pt101:68.

[21] Hötzer J, Rehn V, Rheinheimer W, Hoffmann M, Nestler B. Journal of Ceramic Society of Japan 2016;0pt124:329.

[22] Rheinheimer W, Bäurer M, Handwerker C, Blendell J, Hoffmann M. Acta Materialia 2015;0pt95:111 .

[23] Rheinheimer W, Fülling M, Hoffmann MJ. Journal of the European Ceramic Society 2016;0pt36:2773 .

[24] Jha SK, Raj R. Journal of the American Ceramic Society 2014;0pt97:3103.

[25] Jha SK, Raj R. Journal of the American Ceramic Society 2014;0pt97:527.

[26] M'Peko JC, Francis JSC, Raj R. J Am Ceram Soc 2013;0pt96:3760.

[27] Raj R, Cologna M, Francis JSC. J Am Ceram Soc 2011;0pt94:1941.